Chapter

Effects of Electrolyte Additives on Nonaqueous Redox Flow Batteries

Qian Xu, Chunzhen Yang and Huaneng Su

Abstract

The widespread utilization of nonaqueous redox flow batteries is hindered by the low performance. Including some kinds of additives in electrolyte is a possible and facile solution. In this chapter, the effects of carbon dioxide gas, EC/DMC, and antimony ions on the electrochemical performance of nonaqueous redox flow batteries are disclosed. The results show that the ohmic resistance of the deep eutectic solvent (DES) electrolyte reduces significantly when adding carbon dioxide gas and EC/DMC, the percentage of reduction increases with the volume percentage of EC/DMC in electrolyte, and the reaction kinetics almost keeps unchanged for carbon dioxide gas and EC/DMC additives. For the additive of antimony ions, the electrochemical reaction kinetics of active redox couple is enhanced, the diffusion coefficient of active ions also increases, and the charge transfer resistance decreases. The antimony ions electrodeposited on the surface of graphite felt contribute a catalytic effect on the electrochemical reaction so as to improve the performance. However, due to the trade-off between the enhanced kinetics and reduced active surface area, the optimum concentration of antimony ions is found to be 15 mM. In addition, the flow battery assembled with negative electrolyte containing antimony ions exhibits 31.2% higher power density than that of pristine DES electrolyte.

Keywords: redox flow batteries, deep eutectic solvent (DES), electrolyte additives, carbon dioxide, EC/DMC, antimony ions

1. Introduction

Recent years, with the development of energy storage technology, people prefer to use the redox flow battery (RFB) in large-scale energy storage. RFB has outstanding advantages: it has no limitation by the geographical environment and the sites, the design of cell structure is flexible, and also it shows rapid response to charge and discharge switching and with a long cycle life [1–3]. The aqueous electrolytes for RFB are mostly used during the past decades. However, such systems have a very narrow operating potential window (<2 V) due to the effects of water decomposition which limit the potential power output [4]. In recent years, the research of flow battery technology has extended from aqueous system to nonaqueous system in order to obtain higher potential window. Organic solvents have a much higher electrochemical window, e.g., 5.0 V for acetonitrile (CH_3CN), so that people can gain much higher energy output and power [5]. Even so, organic solvents show potential safety hazards because of their volatility, toxicity, and flammability; moreover, moisture or oxygen contamination can also adversely affect battery performance [6]. To this point, some ionic liquids (ILs) have advantages to solve the problem.

Ionic liquids are salts which can melt at room temperature. These salts have a potential window as wide as organic solvents. Compared with other solvents, ionic liquids have high thermal and electrochemical stability, and the conductivity is higher than aqueous electrolytes [7]. Because of these advantages, ILs have been applied to a lot of fields, such as lithium-ion batteries [8], dye-sensitized solar cells [9], electrolytes in sensors [10], electrochemical capacitors [11], lead acid batteries [12], and fuel cells [13], and even applied to flow batteries recently as electrolyte solutions [14]. In 2015, the applicability of ionic liquids has been explored by Ejigu et al. as solvents of metal complex-containing redox flow battery [15]. Zhang et al. applied $TEAPF_6$ and $EMIPF_6$, two ionic liquids, to nonaqueous redox flow batteries. The results of charge and discharge tests showed that the coulombic efficiencies range from 43.46 to 57.44% [16]. However, there still exist some problems which have become the limitation for their large-scale applications, such as complex synthesis steps, cost, and availability.

The deep eutectic solvent (DES) can be recognized as a peculiar ionic liquid; it is consisting of a conjunction with a stoichiometric ratio of acceptors of hydrogen bond (like quaternary ammonium salts) and donors of hydrogen bond (like compounds of amides, carboxylic acids, and polyols) into the eutectic mixture. We can prepare and use DES under ambient conditions; low cost is the main advantage of DES, which is cheaper than conventional ionic liquids to an order of magnitude; DES is easy to prepare and its overall biodegradability is an advantage too [17–20]. People have carried out preliminary works on the DES. Lloyd et al. had studied the kinetics of electron transfer of the Cu(I)/Cu(II) redox couple with chronoamperometry at a platinum electrode; they named cyclic voltammetry and impedance spectroscopy in a deep eutectic solvent, which consist of choline chloride and ethylene glycol as ethaline [21]. Thereafter, an all-copper hybrid redox flow battery was demonstrated in the ethaline DES [22]. Nevertheless, because of the mass transport limitations and the poor electrolyte conductivity, the energy efficiencies could only reach to 52 and 62% when the current densities were 10 and 7.5 mA cm^{-2}, respectively. In recent researches, the electrochemical and transport characteristics of Fe(II)/Fe(III) as well as V(II)/V(III) redox couples in the DES electrolytes had been studied by Xu group [23, 24].

When people use pristine DES as electrolyte, the main issues are large viscosity and its small diffusion coefficient, which will lead to large pumping loss and cause low efficiency for RFBs [25]. In order to overcome these problems, researchers proposed ways of adding appropriate additives into the electrolyte, like gas and ionic additives, and tuning the active materials by adopting molecular engineering [26, 27]. In 2015, the viscosity changes of ionic liquids after adding SO_2 had been studied by Zeng et al. [27]. The results indicate that when the concentration of SO_2 increases, the viscosity of conventional ionic liquids will decrease sharply. Also, some studies have shown that the adoption of high-pressure CO_2 in DES can certainly improve the physical properties of the RFB system, and this can also increase its electrical conductivity [28–32]. However, there are not too much literature about how the gas additives influence on the electrochemical performance of nonaqueous flow batteries. Moreover, some supporting electrolytes are widely used in lithium-ion batteries for the reduction of electrolyte viscosity as well as the enhancement of cell performance [33], but few are reported in redox flow batteries.

Metal ions are also widely used as additives of electrolytes for electrochemical energy system. Antimony (Sb) has the advantages of low cost, good chemical stability, and high catalytic activity, such that it is widely used in the field of electrocatalysis and battery [23, 34]. In 2015, Shen et al. introduced $SbCl_3$ into a vanadium redox flow battery (VRFB) [35]. The work shows that the added $SbCl_3$ can improve the electrochemical activity and redox kinetics of V(III)/V(II).

In this chapter, the effects of electrolyte additives on nonaqueous redox flow batteries are introduced. The additives include CO_2 gas, ethyl acetate/dimethyl carbonate (EC/DMC) supporting electrolyte, and antimony ions. The effects were studied by means of viscosity test, cyclic voltammetry (CV), electrochemical impedance spectroscopy (EIS), and charge-discharge tests. The results here disclose an effective and convenient approach to improve the cell performance of nonaqueous redox flow batteries.

2. Materials, components, and operation parameters

2.1 Preparation of electrolyte

The DES electrolyte could be prepared by combining choline chloride (Aladdin, 98%) and urea (Sinopharm Reagent 57-13-6, 99%), and the molar ratio is 1:2. The solution at 120°C with a magnetic stirrer is heated and stirred until it formed a colorless and transparent liquid, this mixture is also known as "reline," and the temperature of liquid was also reduced to the room temperature. With long-term placement, the DES would appear some white crystalline precipitate, so it needed to be heated over 50°C in advance of the experiment; this process should proceed on the magnetic stirrer for near 30 minutes, and the rotor's rotation promotes the crystalline precipitate's dissolution. When finishing the experiment, DES should be kept in the sealed glass jar timely to avoid pollution caused by water vapor and oxygen in the air. The active material $FeCl_3$ (Sinopharm Reagent 7705-08-0, 99%) with a concentration of 0.1 mol L^{-1} was added into reline, and the mixture at 120°C was heated and stirred to obtain the electrolyte. Vacuum dried the prepared electrolyte for 24 hours before the start of experiment. Divide the solution into two portions, one portion serving as the pristine and the other one being fed with 0.1 MPa of CO_2 (with the purity of 99.99%). The EC (Macklin 98%) and DMC (Macklin 99%) mixture were prepared by 1:1 vol.% and stirred evenly when adding into the DES electrolyte. For the ion additive, the $SbCl_3$ (99%, Sinopharm Chemical Reagent Co., Ltd.) was added into the negative DES electrolyte at a concentration of 5, 10, 15, and 20 mM, respectively.

2.2 Viscosity measurement

Viscosity measurements were conducted with a "DV-2 + PRO" digital viscometer (Shanghai Nirun Co., Ltd.). The electrolyte was placed on a thermostatic dry heater, and the temperature of the solution was measured by a thermocouple thermometer. When the electrolyte reached the predetermined temperature, measure three times the viscosity at each temperature point, and take the average.

2.3 Electrochemical characterizations

Cyclic voltammetry (CV) and electrochemical impedance spectroscopy (EIS) were operated on Chenhua® CHI600 electrochemical workstation. These measurements used a traditional three-electrode system, its working electrode was a 5-mm-diameter glassy carbon electrode, a platinum electrode was used as counter electrode, and the reference electrode was a saturated calomel electrode together with a salt bridge which was filled with the saturated potassium chloride solution. Before each test, polish the glassy carbon electrode on the deerskin with the 0.2-mm aluminum powder, then place the polished electrode in deionized water, and clean it with ultrasonic waves. The CV scan was performed in the range of −0.7–0.9 V for the electrolyte in the case of with and without CO_2. Before the measurement, purge the electrolyte with nitrogen for 15 minutes in order to remove oxygen which dissolved

in the electrolyte. The CVs were measured at 25, 35, and 45°C, respectively, and at each temperature the CV was tested three times. Simultaneously, in the electrochemical impedance spectroscopy measurements, the sinusoidal excitation voltage suitable for the cells was 5 mV. The frequency was in the range of 0.01 Hz–100 kHz. The potential was settled at 0.15 V in order to ensure similar polarization.

3. Effect of carbon dioxide additive

3.1 Cyclic voltammetry

The cyclic voltammograms of 0.1 M $FeCl_3$ in reline DES at different temperatures with and without 0.1 MPa CO_2 are shown in **Figure 1**. The result indicates that in the range of −0.7–0.9 V with the scan rate of 25 mV s^{-1}, there are two peaks: one is the oxidation peak and the other one is the reduction peak, and the position does not change basically where the peaks appear. For example, in the case of 25°C, the pristine electrolyte's oxidation and reduction peaks appeared at 0.32 and 0.032 V, respectively. After the CO_2 is being introduced, the electrolyte's oxidation peak appeared at 0.318 V and the reduction peak appeared at 0.033 V. This means that the introduction of CO_2 does not affect the electrolyte composition because there is no generation of new material and it does not substantially affect the redox reversibility of the electrolyte. (The physical absorption of CO_2 is also confirmed in reline DES.) On the basis of the redox peak currents, after the CO_2 has been introduced, the peak current does not change significantly. In the case of 25°C, the pristine electrolyte showed the oxidation peak current density of 0.176 mA cm^{-2}, and in this case, the reduction peak

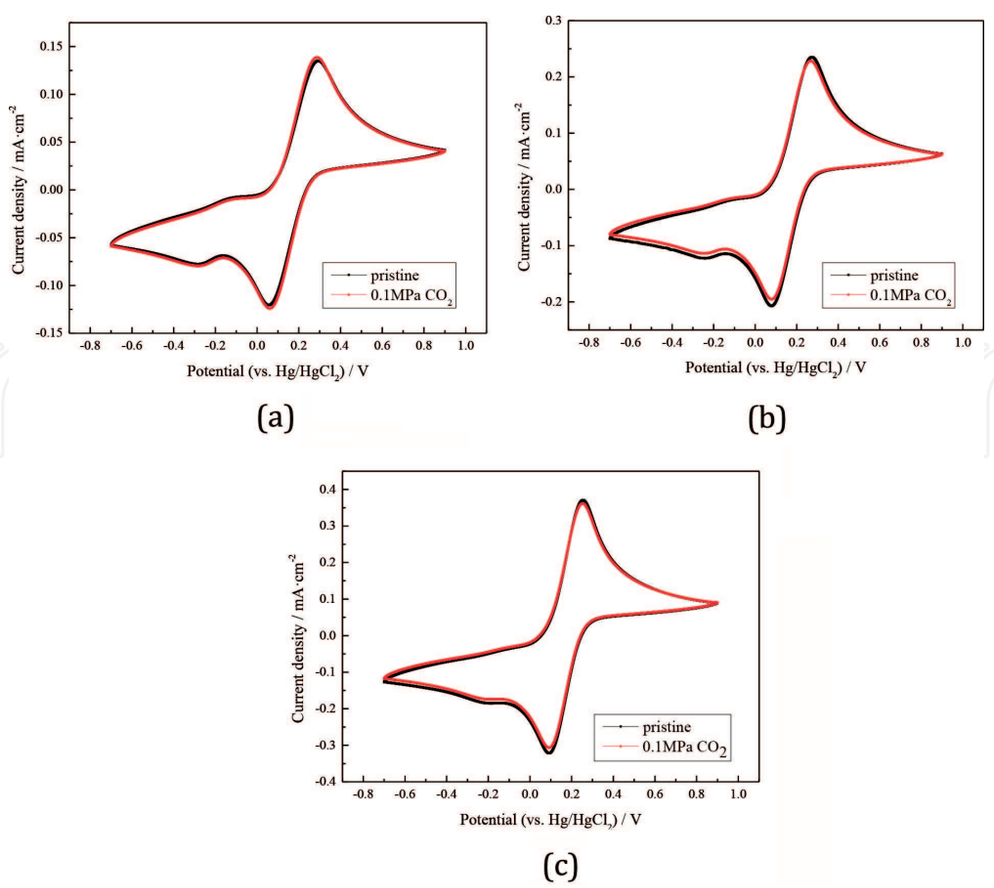

Figure 1.
Cyclic voltammograms of 0.1 M $FeCl_3$ in reline DES with and without 0.1 MPa CO_2 at different temperatures: (a) 25°C, (b) 35°C, and (c) 45°C.

current density was −0.158 mA cm^{-2}. After introducing CO_2, they became 0.178 and − 0.16 mA cm^{-2}, respectively. The result shows that the rate of redox reaction of Fe(II)/Fe(III) redox couple in DES changes little when CO_2 is being added in.

3.2 Electrochemical impedance spectroscopy

Electrochemical impedance spectroscopy (EIS) was carried out to further investigate how the addition of CO_2 influences the electrochemical performance of Fe(III) ion in DES electrolyte. The Nyquist plots of Fe(III) in DES electrolyte at different temperatures with and without CO_2 are shown in **Figure 2**. Each plot shows a similar illustration: in the high-frequency region, there is a semicircle and in the low-frequency region, there is a straight line upward. They correspond to the transfer reaction of charge at the interface of electrode/electrolyte and the diffusion of iron species in the electrolyte, respectively, and this result suggests that electrochemical reaction and diffusion steps mix-control the Fe(III)/Fe(II) redox reaction [36]. There is a distance from the crossing of the semicircle's left end and the abscissa to the origin, which is the ohmic resistance of the electrolyte, and the semicircle's diameter is the electrochemical reaction resistance of the electrolyte. In order to determine the ohmic resistance and the electrochemical reaction resistance precisely before and after adding 0.1 MPa CO_2 to the reline DES which contains 0.1 M $FeCl_3$ in case of different temperatures, the data were fitted and the straight line in **Figure 2** showed the results. **Figure 2** shows a simplified equivalent circuit; the resistance of the ion migration process in the solution is represented as *Rs*, that is to say, the ohmic resistance of the solution. *Rt* is the resistance of electrochemical reaction, the resistance of the electron transfer step. *CPE* represents

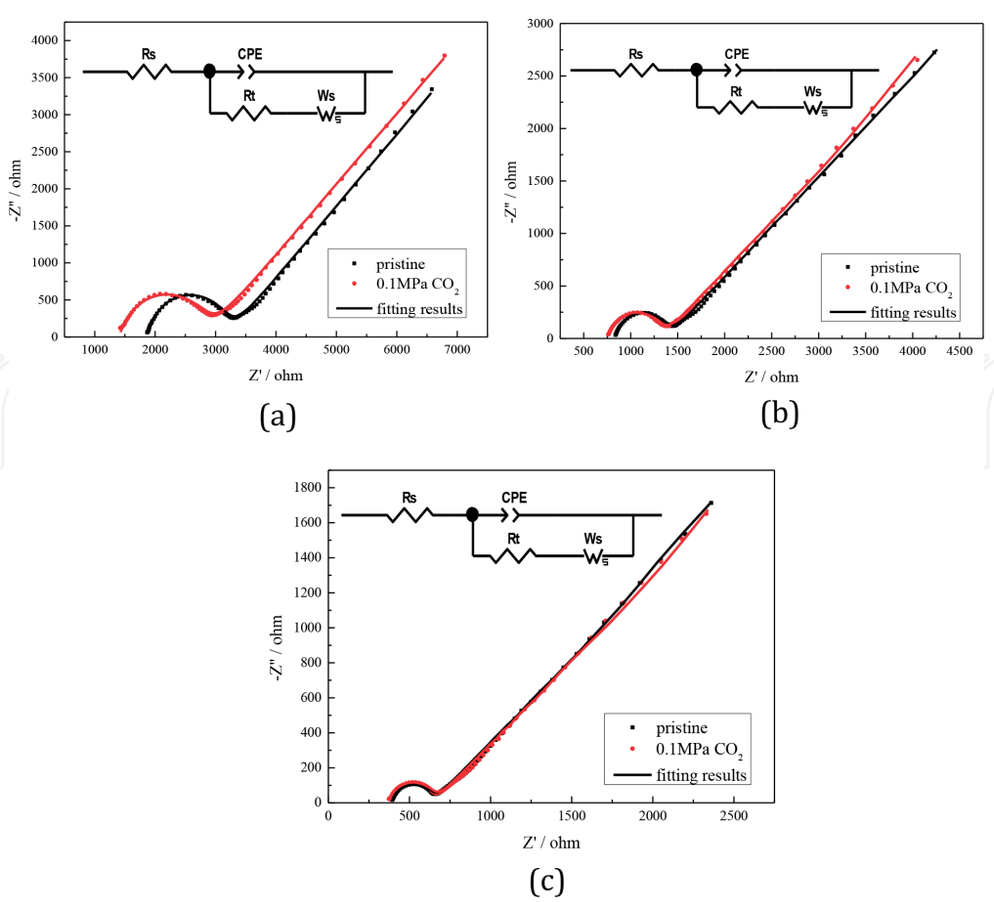

Figure 2.
Nyquist plots of the electrolyte with and without CO_2 at different temperatures and the corresponding equivalent circuit: (a) 25°C, (b) 35°C, and (c) 45°C.

Temperature (°C)	*Rs* (ohm)		*Rt* (ohm)	
	Pristine	0.1 MPa CO_2	Pristine	0.1 MPa CO_2
25	1867	1409	1337	1446
35	834.7	757.5	560.6	587.3
45	390.2	373.2	251.3	277.8
55	233.6	227.6	129.3	149

Table 1.
The parameters obtained from fitting the EIS plots with the equivalent circuit for carbon dioxide additive.

the double-layer capacitance of the interface, simulating the process of the double layer in case of charge and discharge. *Ws* stands for the concentration polarization impedance, which simulates the liquid phase's mass transfer.

The Z-view simulation helps to obtain the parameters of the equivalent circuit, which are listed in **Table 1**. It can be found that the resistance *Rs* of the electrolyte decreases after the addition of 0.1 MPa CO_2. In detail, at the temperature of 25°C, it decreases from 1867 to 1409 ohm. The solubility of CO_2 in the electrolyte will decrease when the temperature increases, so the decline percentage of *Rs* becomes small, and it is consistent with the trend of viscosity. What is more, the electrochemical reaction resistance of the solution slightly increases, implying that the addition of CO_2 would slow down the charge transfer process of the electrolyte solution. The redox flow battery with DES electrolyte adding CO_2 has a little-changed overall performance compared with the pristine DES electrolyte.

4. Effect of EC/DMC supporting electrolyte

4.1 Cyclic voltammetry

The cyclic voltammograms of 0.1 M $FeCl_3$ in reline DES without and with EC/DMC are shown in **Figure 3**. The volume of the tested DES electrolyte is 40 ml. The result indicates that with the scan rate of 50 mV s^{-1} in the range of −0.7–1.2 V, there appear only one oxidation peak and only one reduction peak. The position of the peak does not distinctly change with the addition of EC/DMC. After the introduction of EC/DMC (4 ml, 10% vol.), the oxidation peak and the reduction peak shift left and right for <50 mV, respectively. This suggests that the introduction of EC/DMC neither affects the electrolyte composition nor substantially affects the redox reversibility of the electrolyte. In terms of the redox peak currents, after the introduction of EC/DMC, the peak current increases for <10%. The result implies that the rate of redox reaction of Fe(II)/Fe(III) redox couple in DES does not change remarkably with the addition of EC/DMC.

4.2 Electrochemical impedance spectroscopy

The Nyquist plots of Fe(III) in DES electrolyte with and without EC/DMC are shown in **Figure 4**. For the pristine DES, the plot shows a semicircle in the high-frequency region, and in the low-frequency region, there is a straight line upward; the semicircle corresponds to the charge transfer reaction at the electrode/electrolyte interface, and the straight line upward corresponds to the diffusion of iron species in the electrolyte, suggesting electrochemical reaction and diffusion steps mix-control the Fe(III)/Fe(II) redox reaction. With the addition of EC/DMC,

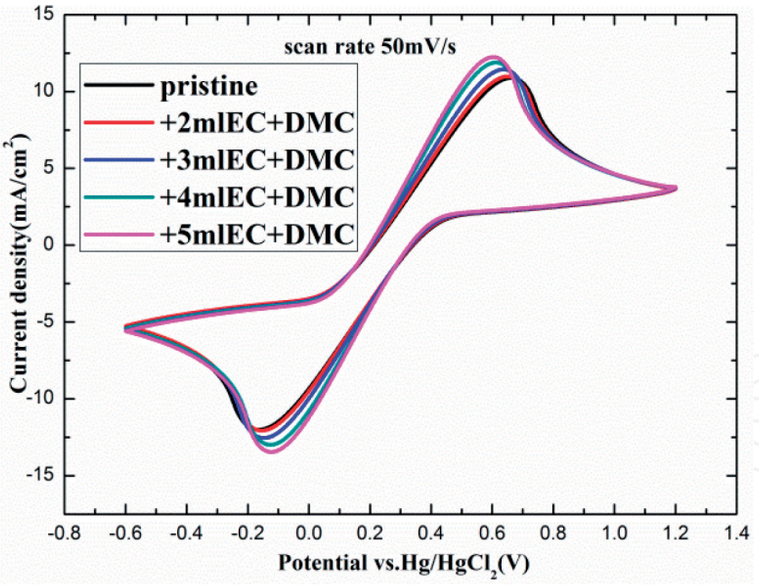

Figure 3.
CV curves of different concentrations of EC/DMC additive in DES with 0.1 mol L^{-1} $FeCl_3$ with a scan rate of 50 mV s^{-1}.

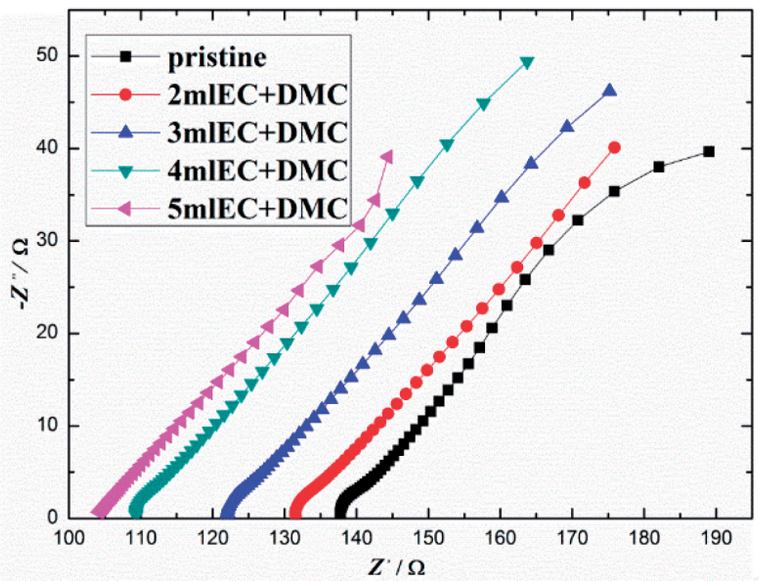

Figure 4.
AC impedance spectra for different concentrations of EC/DMC in DES with 0.1 mol L^{-1} $FeCl_3$.

the radius of semicircle reduces, suggesting the charge transfer reaction becomes diffusion-controlled. With addition of more EC/DMC, the ohmic resistance (*Rs*) of the DES electrolyte becomes smaller. For example, for the pristine DES, the *Rs* is 137.9 Ω; for the electrolyte with 3 ml EC/DMC, it is 122.2 Ω; and for the DES with 5 ml EC/DMC, it reduces to 103.4 Ω. The electrochemical reaction resistance (*Rt*) almost keeps unchanged with the addition of EC/DMC.

The Raman spectroscopy shows that the introduction of EC/DMC does not change the shape of spectrum significantly (**Figure 5**). The peak near 3000 cm^{-1} is a result of the overlap of the characteristic peaks of choline chloride and ethylene glycol (the main components of DES), while a new characteristic peak appears around 895 cm^{-1} when EC/DMC is added into the DES electrolyte, which can be attributed to the symmetrical stretching vibration of C-O-C bond when aliphatic ethers exist in the nonaqueous solution [33]. The reduction of ohmic resistance after the addition of EC/DMC should be the result of the stretching vibration of C-O-C bond.

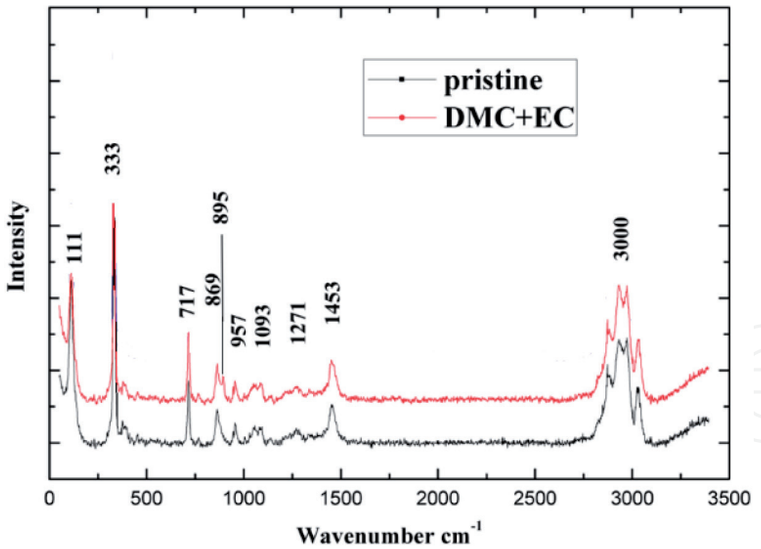

Figure 5.
Raman spectra of solvents without and with EC/DMC additive.

5. Effect of antimony ions

Inspired by the use of antimony ions as the additive in VRFBs, the same ions are tried to be the additive in DES electrolyte nonaqueous RFBs. The active materials used in negative side electrolyte are V(III)/V(II) redox ions.

5.1 Cyclic voltammetry

The cyclic voltammetry curves of negative electrolyte containing 0.1 mol L^{-1} VCl_3 with different concentrations of $SbCl_3$ are shown in **Figure 6**, and the scanning rate is 25 mV s^{-1}. It shows two obvious peaks corresponding to V(III)/V(II) redox couple. A small peak appears at the position of −0.2 V, and since there is no peak in DES, thus the small peak at −0.2 V should be caused by impurities in the raw materials. In addition, there is no new peak, which further proves that after

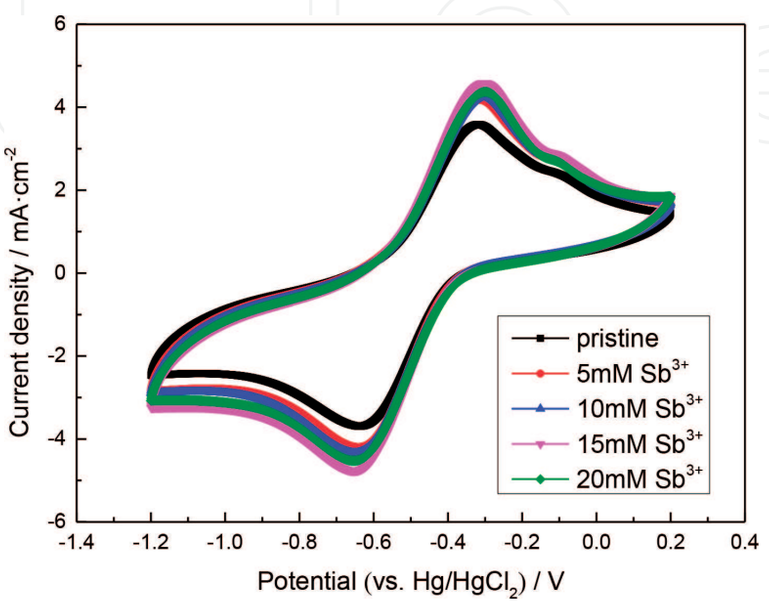

Figure 6.
Effect of Sb^{3+} on CV curves of 0.1 M VCl_3 in DES at the scanning rate of 25 mV s^{-1}.

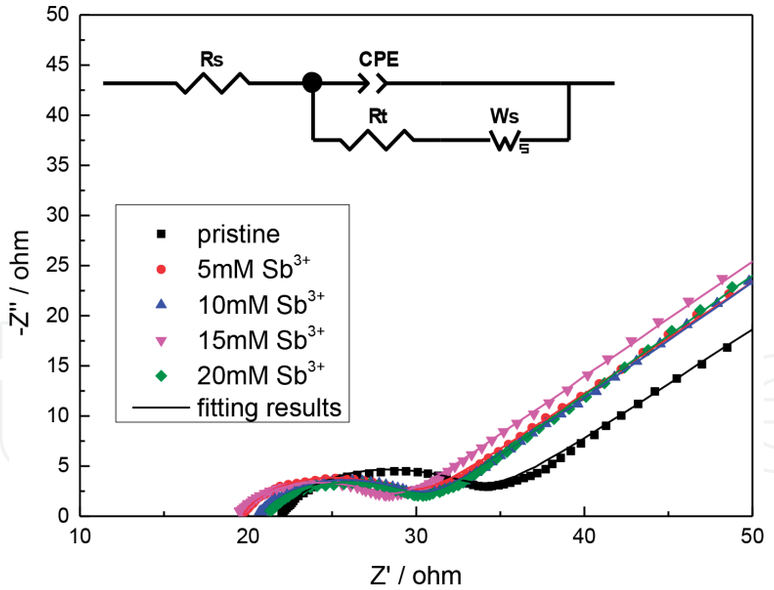

Figure 7.
Nyquist plot of 0.1 M VCl_3 in DES with different concentrations of Sb^{3+} ions.

the addition of Sb^{3+} ions, there is no chemical reaction with V(III) ions to generate a new substance. For the pristine electrolyte, the peak current densities were 3.583 and −3.691 mA cm^{-2}, respectively. After the introduction of Sb^{3+} ions, both of them increase and reach the maximum (4.589 and −4.764 mA cm^{-2}, respectively) when the concentration of Sb^{3+} ions is 15 mM. This indicates that the introduction of Sb^{3+} ions can accelerate the redox reaction rate of the battery and increase the collision between ions which makes it easier to overcome the activation energy and realize the electrochemical reaction [37].

5.2 Electrochemical impedance spectroscopy

The influence of $SbCl_3$ on the electrochemical properties of negative electrolyte was further investigated by EIS. The Nyquist plots of electrolyte without additive and with different concentration of $SbCl_3$ are shown in **Figure 7**. The combination of semicircle and the straight line upward suggests that the redox reaction of vanadium is mix-controlled by electrochemical polarization and concentration polarization [38]. **Figure 5** shows the corresponding simplified equivalent circuit, where *Ws* and *CPE* represent the concentration polarization impedance and double-layer capacitance of the solution, respectively.

It can be seen that the *Rs* and *Rt* of electrolyte decrease with the addition of different concentrations of $SbCl_3$ and reach the minimum when the concentration is 15 mM. The corresponding parameters of the equivalent circuit obtained by the Z-view simulation are shown in **Table 2**. The *Rs* and *Rt* of the solution with 15 mM $SbCl_3$ were the smallest; they were 19.41 and 8.95 ohm cm^{-2}, respectively, lower than that of the pristine electrolyte (22.03 and 11.57 ohm m^{-2}). The reduced electrochemical reaction resistance indicates that the charge transfer process of the electrolyte is accelerated, which reflects the higher electrochemical reaction rate. This is probably owing to the adhesion of Sb to the electrode and its catalytic effect. The increased *CPE* and *Ws* suggest that the Sb^{3+} in the electrolyte is able to promote the absorption and diffusion of V ions. The results further confirm that the addition of Sb^{3+} can improve the electrochemical reaction of V(III)/V(II).

In order to investigate the influence of the addition of $SbCl_3$ on the power density of the battery, the polarization curve of the flow battery was measured (the active material is $FeCl_3$ in positive side electrolyte). As shown in **Figure 8**, when

Concentration of Sb^{3+}	*Rs* (ohm cm^{-2})	*Rt* (ohm cm^{-2})	*CPE* (F cm^{-2})	*Ws*
Pristine	22.03	11.57	7.218×10^{-4}	0.5338
5 mM	20.72	9.89	9.86×10^{-4}	0.5381
10 mM	20.67	9.50	1.01×10^{-3}	0.5478
15 mM	19.41	8.95	1.15×10^{-3}	0.5581
20 mM	21.15	9.11	1.06×10^{-3}	0.5492

Table 2.
The parameters obtained from fitting the EIS plots with the equivalent circuit for antimony ion additive.

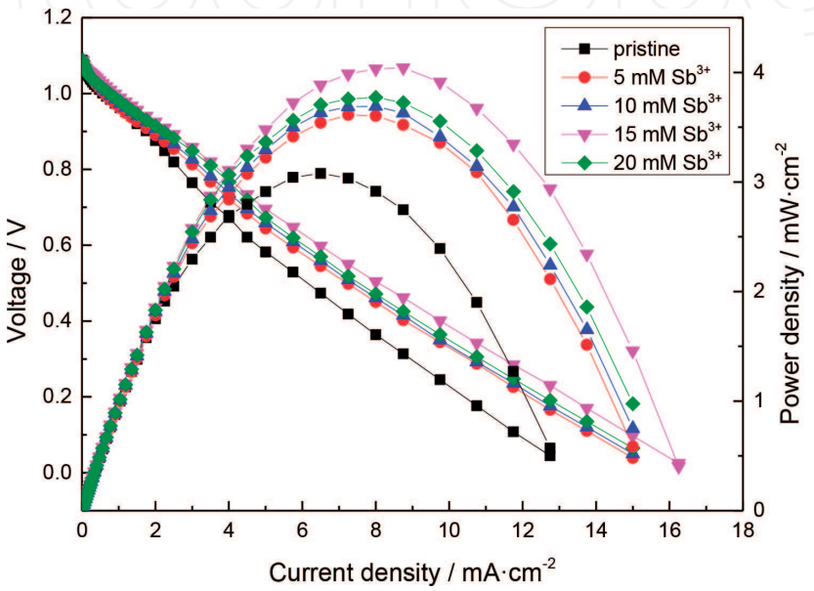

Figure 8.
Polarization curves of batteries with different concentrations of Sb^{3+} ions.

the concentration of Sb^{3+} ions increases, the maximum current density and maximum power density increase first and then decrease, and when the concentration reached 15 mM, they reached the maximum (16.25 mA cm^{-2} and 4.04 mW cm^{-2}, respectively), higher than those of pristine electrolyte (12.75 mA cm^{-2} and 3.08 mW cm^{-2}). From these experimental results, it can be seen that the electrochemical performance of V(III)/V(II) redox couple has been improved due to the adhesion of Sb ion to the electrode and its catalytic effect.

5.3 Physicochemical measurements

To explore the mechanism of Sb ions to improve the electrochemical performance of electrolytes, the surface morphology of graphite felts obtained after charging-discharging cycle was characterized by SEM. **Figure 9** shows that some particles adhere to the surface of graphite felt after the addition of $SbCl_3$.

With the increased concentration of $SbCl_3$, the particles on the surface of graphite felt increased. In order to analyze the specific composition of the observed ions, the energy-dispersive X-ray spectroscopy (EDX) was used to identify them. As shown in **Figure 10**, the transverse coordinate is the energy, and the vertical coordinate is the relative content of elements. The results of EDX show that the elements on the pristine surface of graphite felt are only C, O, V, and Cl and the particle detected after the addition of additives is Sb. Corresponding to the energy of 4.0 keV, the content of Sb on graphite felt increases gradually with the increased concentration of

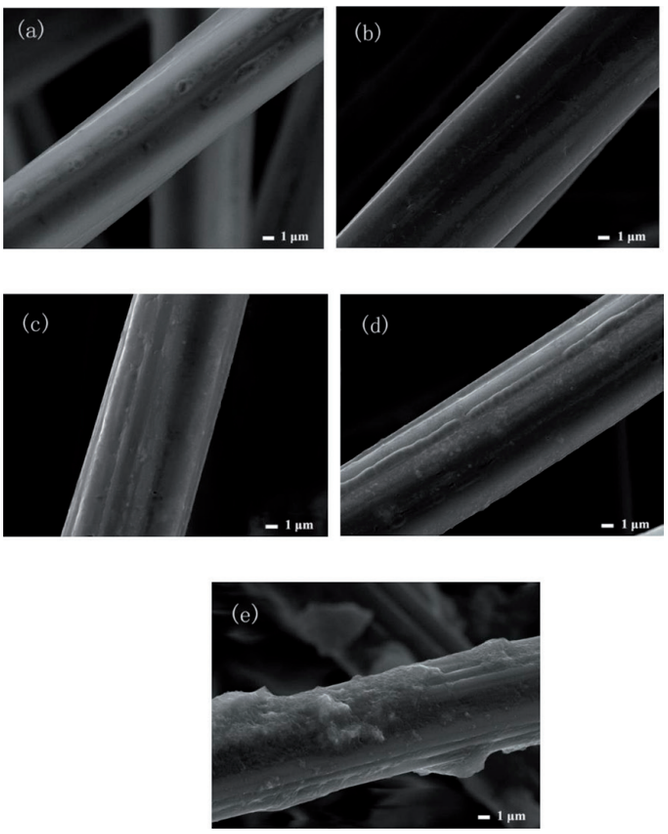

Figure 9.
The FESEM images of graphite felt electrode after cycling: (a) pristine, (b) 5 mM Sb^{3+}, (c) 10 mM Sb^{3+}, (d) 15 mM Sb^{3+}, and (e) 20 mM Sb^{3+}.

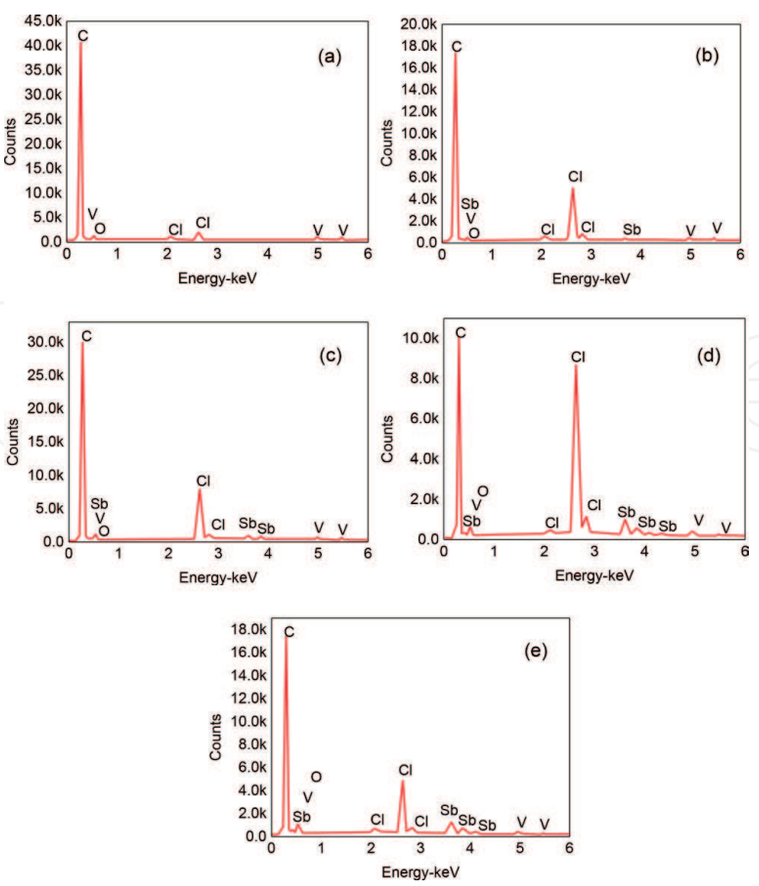

Figure 10.
EDX spectrogram of ions on the surface of graphite felts: (a) pristine, (b) 5 mM Sb^{3+}, (c) 10 mM Sb^{3+}, (d) 15 mM Sb^{3+}, and (e) 20 mM Sb^{3+}.

$SbCl_3$. The results suggest that the enhancement of the battery performance is owing to the catalytic effect of Sb ions. However, when the concentration was 20 mM, the accumulation of ions is more serious, which would result in partial pore blockage of graphite felt. Therefore, when the concentration of Sb^{3+} ions further increases, the electrochemical performance of the battery decreases slightly.

6. Conclusions

The effects of three kinds of additives including carbon dioxide gas, EC/DMC, and Sb^{3+} ions on the electrochemical performance of nonaqueous DES electrolyte redox flow batteries are explored. The ohmic resistance of the deep eutectic solvent (DES) electrolyte decreases significantly when adding carbon dioxide gas and EC/DMC, and the percentage of reduction increases with the volume percentage of EC/DMC in electrolyte, while for these two additives, the reaction kinetics almost keeps unchanged.

With CO_2 in DES, the electrochemical reaction resistance increases about 10%. For EC/DMC additive, the electrochemical reaction resistance almost keeps the same no matter the amount of additive in electrolyte. For the additive of Sb^{3+} ions in DES electrolyte, the electrochemical reaction kinetics of active redox couple is enhanced, the diffusion coefficient of active ions increases, and the charge transfer resistance decreases. The electrodeposited Sb^{3+} ions on electrode surface contribute a catalytic effect on the electrochemical reaction. However, due to the trade-off between the enhanced kinetics and reduced active surface area, the optimum concentration of Sb^{3+} ions is found to be 15 mM. In addition, the flow battery assembled with negative electrolyte containing Sb^{3+} ions exhibits 31.2% higher power density. The results in this chapter provide a simple yet effective approach to promote the cell performance of nonaqueous redox flow batteries.

Acknowledgements

The work described in this chapter was fully supported by grants from the NSFC, China (No. 51676092 and No. 21676126), Six Talent Peaks Project in Jiangsu Province (2016-XNY-015), and a project funded by the Priority Academic Program Development (PAPD) of Jiangsu Higher Education Institutions, China.

Conflict of interest

There is no conflict of interest to be declared.

Author details

Qian Xu[1*], Chunzhen Yang[2] and Huaneng Su[1]

1 Institute for Energy Research, Jiangsu University, Zhenjiang, China

2 School of Materials Science and Engineering, Sun Yat-Sen University, Guangzhou, China

*Address all correspondence to: xuqian@ujs.edu.cn

References

[1] Leung P, Li X, De Leon CP, et al. Progress in redox flow batteries, remaining challenges and their applications in energy storage. RSC Advances. 2012;**2**(27):10125-10156. DOI: 10.1039/c2ra21342g

[2] Alotto P, Guarnieri M, Moro F. Redox flow batteries for the storage of renewable energy: A review. Renewable and Sustainable Energy Reviews. 2014;**29**: 325-335. DOI: 10.1016/j.rser.2013.08.001

[3] Soloveichik GL. Flow batteries: Current status and trends. Chemical Reviews. 2015;**115**(20):11533-11558. DOI: 10.1021/cr500720t

[4] Chakrabarti MH, Dryfe RAW, Roberts EPL. Evaluation of electrolytes for redox flow battery applications. Electrochimica Acta. 2007;**52**(5):2189-2195. DOI: 10.1016/j.electacta.2006.08.052

[5] Low CTJ, Walsh FC, Chakrabarti MH, et al. Electrochemical approaches to the production of graphene flakes and their potential applications. Carbon. 2013;**54**(4):1-21. DOI: 10.1016/j.carbon.2012.11.030

[6] Escalante-García IL, Wainright JS, Thompson LT, et al. Performance of a non-aqueous vanadium acetylacetonate prototype redox flow battery: Examination of separators and capacity decay. Journal of the Electrochemical Society. 2015;**162**(3):A363-A372. DOI: 10.1149/2.0471503jes

[7] Leung PK, Sanz L, Flox C, Xu Q, Shah AA, Walsh FC. Recent developments in organic redox flow batteries: A critical review. Journal of Power Sources. 2017;**360**:243-282. DOI: 10.1016/j.jpowsour.2017.05.057

[8] Lewandowski A, Swiderska-Mocek A. ChemInform abstract: Ionic liquids as electrolytes for li-ion batteries: An overview of electrochemical studies. ChemInform. 2010;**41**(38):601-609. DOI: 10.1016/j.jpowsour.2009.06.089

[9] Jhong HR, Wong SH, Wan CC, et al. A novel deep eutectic solvent-based ionic liquid used as electrolyte for dye-sensitized solar cells. Electrochemistry Communications. 2009;**11**(1):209-211. DOI: 10.1016/j.elecom.2008.11.001

[10] Wei D, Ivaska A. Applications of ionic liquids in electrochemical sensors. Analytica Chimica Acta. 2008;**607**(2):126-135. DOI: 10.1016/j.aca.2007.12.011

[11] Lu W, Qu L, Henry K, et al. High performance electrochemical capacitors from aligned carbon nanotube electrodes and ionic liquid electrolytes. Journal of Power Sources. 2009;**189**(2):1270-1277. DOI: 10.1016/j.jpowsour.2009.01.009

[12] Rezaei B, Mallakpour S, Taki M. Application of ionic liquids as an electrolyte additive on the electrochemical behavior of lead acid battery. Journal of Power Sources. 2009;**187**(2):605-612. DOI: 10.1016/j.jpowsour.2008.10.081

[13] Souza RF, Padilha JC, Gonçalves RS, et al. Room temperature dialkylimidazolium ionic liquid-based fuel cells. Electrochemistry Communications. 2003;**5**(8):728-731. DOI: 10.1016/s1388-2481(03)00173-5

[14] Chakrabarti MH, Mjalli FS, AlNashef IM, et al. Prospects of applying ionic liquids and deep eutectic solvents for renewable energy storage by means of redox flow batteries. Renewable and Sustainable Energy Reviews. 2014;**30**:254-270. DOI: 10.1016/j.rser.2013.10.004

[15] Ejigu A, Greatorex-Davies PA, Walsh DA. Room temperature ionic liquid electrolytes for redox flow batteries. Electrochemistry Communications. 2015;**54**:55-59. DOI: 10.1016/j.elecom.2015.01.016

[16] Ding Y, Zhang C, Zhang L, Zhou Y, Yu G. Molecular engineering of organic electroactive materials for redox flow batteries. Chemical Society Reviews. 2018;**47**:69-103. DOI: 10.1039/C7CS00569E

[17] Bahadori L, Hashim MA, Manan NSA, et al. Investigation of ammonium- and phosphonium-based deep eutectic solvents as electrolytes for a non-aqueous all-vanadium redox cell. Journal of the Electrochemical Society. 2016;**163**(5):A632-A638. DOI: 10.1149/2.0261605jes

[18] Miller MA, Wainright JS, Savinell RF. Iron electrodeposition in a deep eutectic solvent for flow batteries. Journal of the Electrochemical Society. 2017;**164**(4):A796-A803. DOI: 10.1149/2.1141704jes

[19] Zhang C, Ding Y, Zhang L, Wang X, Zhao Y, Zhang X, et al. A sustainable redox-flow battery with an aluminum-based deep-eutectic-solvent anolyte. Angewandte Chemie, International Edition. 2017;**56**:7454-7459. DOI: 10.1002/ange.201703399

[20] Zhang L, Zhang C, Ding Y, Ramirez-Meyers K, Yu G. A low-cost and high-energy hybrid iron-aluminum liquid battery achieved by deep eutectic solvents. Joule. 2017;**1**:623-633. DOI: 10.1016/j.joule.2017.08.013

[21] Lloyd D, Vainikka T, Murtomaki L, et al. The kinetics of the Cu^{2+}/Cu^{+} redox couple in deep eutectic solvents. Electrochimica Acta. 2011;**56**(14):4942-4948. DOI: 10.1016/j.electacta.2011.03.133

[22] Lloyd D, Vainikka T, Kontturi K. The development of an all copper hybrid redox flow battery using deep eutectic solvents. Electrochimica Acta. 2013;**100**:18-23. DOI: 10.1016/j.electacta.2013.03.130

[23] Xu Q, Zhao TS, Wei L, Zhang C, Zhou XL. Electrochemical characteristics and transport properties of Fe(II)/Fe(III) redox couple in a non-aqueous reline deep eutectic solvent. Electrochimica Acta. 2015;**154**:462-467. DOI: 10.1016/j.electacta.2014.12.061

[24] Xu Q, Qin LY, Su HN, Xu L, Leung PK, Yang CZ, et al. Electrochemical and transport characteristics of V(II)/V(III) redox couple in a nonaqueous reline deep eutectic solvent: Temperature effect. Journal of Energy Engineering. 2017;**143**(5):04017051. DOI: 10.1016/j.electacta.2014.12.061

[25] Zhang C, Zhang L, Ding Y, Peng S, Guo X, Zhao Y, et al. Progress and prospects of next-generation redox flow batteries. Energy Storage Materials. 2018;**15**:324-350. DOI: 10.1016/j.ensm.2018.06.008

[26] Ding Y, Yu G. The promise of environmentally benign redox flow batteries by molecular engineering. Angewandte Chemie, International Edition. 2017;**56**:8614-8616. DOI: 10.1002/anie.201701254

[27] Zeng S, Zhang X, Gao H, et al. SO_2-induced variations in the viscosity of ionic liquids investigated by in situ fourier transform infrared spectroscopy and simulation calculations. Industrial and Engineering Chemistry Research. 2015;**54**(43):10854-10862. DOI: 10.1021/acs.iecr.5b01807

[28] Li X, Hou M, Han B, et al. Solubility of CO_2 in a choline chloride^{+} urea eutectic mixture. Journal of Chemical and Engineering Data. 2008;**53**(2):548-550. DOI: 10.1021/je700638u

[29] Leron RB, Li MH. High-pressure volumetric properties of choline chloride-ethylene glycol based deep eutectic solvent and its mixtures with water. Thermochimica Acta. 2012;**546**:54-60. DOI: 10.1016/j.tca.2012.07.024

[30] Leron RB, Li MH. High-pressure density measurements for choline chloride: Urea deep eutectic solvent and its aqueous mixtures at T = (298.15 to 323.15) K and up to 50 MPa. The Journal of Chemical Thermodynamics. 2012;**54**:293-301. DOI: 10.1016/j.jct.2012.05.008

[31] Ali E, Hadj-Kali MK, Mulyono S, et al. Solubility of CO_2, in deep eutectic solvents: Experiments and modelling using the Peng–Robinson equation of state. Chemical Engineering Research and Design. 2014;**92**(10):1898-1906. DOI: 10.1016/j.cherd.2014.02.004

[32] Haghbakhsh R, Raeissi S. Modeling the phase behavior of carbon dioxide solubility in deep eutectic solvents with the cubic plus association equation of state. Journal of Chemical and Engineering Data. 2018;**63**(4):897-906. DOI: 10.1021/acs.jced.7b00472

[33] Wiercigroch E, Szafraniec E, Czamara K, et al. Raman and infrared spectroscopy of carbohydrates: A review. Spectrochimica Acta Part A: Molecular and Biomolecular Spectroscopy. 2017;**185**:317-335. DOI: 10.1016/j.saa.2017.05.045

[34] Xu Q, Qin LY, Su HN, Xu L, Leung P, Yang C. Electrochemical and transport characteristics of V(II)/V(III) redox couple in a nonaqueous deep eutectic solvent: Temperature effect. Journal of Energy Engineering. 2017;**143**:04017051. DOI: 10.1061/(ASCE)EY.1943-7897.0000484

[35] Jiang HR, Zeng YK, Wu MC. A uniformly distributed bismuth nanoparticle-modified carbon cloth electrode for vanadium redox flow batteries. Applied Energy. 2019;**240**:226-235. DOI: 10.1016/j.apenergy.2019.02.051

[36] Shen J, Liu S, He Z, et al. Influence of antimony ions in negative electrolyte on the electrochemical performance of vanadium redox flow batteries. Electrochimica Acta. 2015;**151**:297-305. DOI: 10.1016/j.electacta.2014.11.060

[37] Skyllas-Kazacos M, Chakrabarti MH, Hajimolana SA, Mjalli FS, Saleem M. Progress in flow battery research and development. Journal of the Electrochemical Society. 2015;**158**:R55-R79. DOI: 10.1149/1.3599565

[38] Xu Q, Ji YN, Qin LY, Leung PK, Shah AA, Li YS. Effect of carbon dioxide additive on the characteristics of a deep eutectic solvent (DES) electrolyte for non-aqueous redox flow batteries. Chemical Physics Letters. 2018;**708**:48-53. DOI: 10.1016/j.cplett.2018.07.060